Title

Electric-field control of tri-state phase transformation with a selective dual-ion switch

Journal

Nature, 546(7656)

ISSN

0028-0836

Authors

Lu, Nianpeng

Zhang, Pengfei

Zhang, Qinghua

et al.

Publication Date

2017-06-01

DOI

10.1038/nature22389

Peer reviewed

Electric-field control of tri-state phase transformation with selective dual-ion switch

Nianpeng Lu[1], Pengfei Zhang[1], Qinghua Zhang[2, 3], Ruimin Qiao[4], Qing He[5], Haobo Li[1], Yujia Wang[1], Jingwen Guo[1], Ding Zhang[1], Zheng Duan[1], Zhuolu Li[1], Meng Wang[1], Shuzhen Yang[1], Mingzhe Yan[1], Elke Arenholz[4], Shuyun Zhou[1, 6], Wanli Yang[4], Lin Gu[2, 6], Cewen Nan[3], Jian Wu[1, 6*], Yoshi Tokura[7] and Pu Yu[1, 6, 7*]

[1]State Key Laboratory of Low Dimensional Quantum Physics and Department of Physics, Tsinghua University, Beijing 100084, China

[2]Beijing National Laboratory for Condensed Matter Physics, Institute of Physics, Chinese Academy of Science, Beijing 100190, China

[3]State Key Lab of New Ceramics and Fine Processing, School of Materials Science and Engineering, Tsinghua University, Beijing, 100084 China

[4]Advanced Light Source, Lawrence Berkeley National Laboratory, Berkeley, California 94720, USA

[5]Department of Physics, Durham University, Durham DH1 3LE, United Kingdom

[6]Collaborative Innovation Center of Quantum Matter, Beijing, China

[7]RIKEN Center for Emergent Matter Science (CEMS), Saitama, Japan

[*]Correspondence to: wu@tsinghua.edu.cn and yupu@tsinghua.edu.cn

Electric-field control of phase transformation with ion transfer is of great interest in materials science with enormous practical applications, such as batteries[1], smart windows[2], fuel cells[3], etc. Although increasing numbers of the transport ion species and the corresponding controllable crystalline phases can greatly enrich the material functionalities, studies have so far targeted mainly by the evolution of single ionic species (e.g. O^{2-}, H^{+}, Li^{+}, etc.) [4-10]. Here we report the reversible and nonvolatile electric-field control of dual-ion (with both O^{2-} and H^{+}) phase transformation with the discovery of the exotic tri-state electrochromic[2] and magnetoelectric[11] effects. With the independently controllable O^{2-} and H^{+} ion insertion and extraction, we realize the reversible phase transformation among *three* phases – the perovskite $SrCoO_{3-\delta}$[12], brownmillerite $SrCoO_{2.5}$[13] and a hitherto-unexplored $SrCoO_{2.5}H$. Due to their distinct optical absorption, we demonstrate a selective manipulation of the spectra optical transparency among the visible-light and infrared regions, revealing a fascinating dual-band electrochromic effect with promising applications in smart windows[2, 9]. Moreover, the stark different magnetic and electric properties of $SrCoO_{2.5}H$ (ferromagnetic insulator) as compared with $SrCoO_{3-\delta}$ (ferromagnetic metal)[12] and $SrCoO_{2.5}$ (antiferromagnetic insulator)[13] reveal an intriguing concept of tri-state magnetoelectric coupling with the deterministic electric-field control of the three different magnetic ground states. These findings open up new opportunities for the electric-field control of multi-state phase transformation with novel

crystalline structures and rich functionalities.

Among all the possible anions and cations, the oxygen and hydrogen ions provide the most accessible and effective pathways for inducing the phase transformation with novel electronic and magnetic properties. Although this transformation can be achieved conventionally with thermal annealing[12-18], the electric field control has unique advantages due to its excellent accessibility and tunability with extended functionalities[4-8]. In recent years, the electronic-field controllable ionic liquid gating (ILG) has emerged as an attractive controlling knob for manipulating material properties not only through well-established electrostatic doping[19-21], but also by inducing phase transformation with ion transfer through its intrinsic electrochemical effect[22]. It has been reported that the ILG can induce either oxygen anion[4] or hydrogen cation[7, 8] evolution in some material systems, as schematically demonstrated in **Figures 1a, b**, while the selective control of bipolar (with both O^{2-} and H^{+}) ion switch has yet to be explored. Here we demonstrate for the first time a reversible and nonvolatile electric-field controlled tri-state phase transformation among three distinct crystalline structures through the dual-ion (both O^{2-} and H^{+}) switch (**Figure 1c**).

The brownmillerite $SrCoO_{2.5}$ was carefully selected as the model system in this study due to the facts that its well-ordered oxygen vacancy channels and multivalent Co ions[13] provide the most favorable condition for the ionic diffusion[23] and valence change[5, 12] for the phase transformation. Our experiments were performed on high-quality epitaxial $SrCoO_{2.5}$ thin films grown on $(LaAlO_3)_{0.3}$-$(SrAl_{0.5}Ta_{0.5}O_3)_{0.7}$ (001) (LSAT) substrate by pulsed laser deposition. The excellent crystalline quality of the as-grown samples were confirmed with the high-resolution X-ray diffraction (XRD, green curve in **Figure 1d**), reciprocal space mapping (RSM) and rocking curve (**Extended Data Figures 1a, b**) measurements.

To provide direct evidence of the structural transition between different phases, we first performed *In-situ* XRD measurements during the ionic liquid gating (**methods**). **Figure 1e** shows the evolution of the characteristic diffraction peaks upon a closed loop of positive and negative gating voltages. The gating voltages were selected based on a systematic analysis of the phase transformations with different gating voltages

(**Extended Figures 2a-h**). With the positive gating of +3.5 V, the (008) diffraction peak (~45.7°) of the brownmillerite phase diminishes gradually and eventually disappears, and a new diffraction peak at ~44.0° starts to develop, suggesting the emergence of a new phase (denoted as "phase A" temporarily). By reversing the gating voltage to -2.3 V, the system can be reverted back to the brownmillerite $SrCoO_{2.5}$ phase, and then further increase the negative gating voltage to -2.7 V can transform the system into the perovskite $SrCoO_{3-\delta}$ phase with the characteristic diffraction peak (002) at ~47.7°. More interestingly, the transformation between the brownmillerite and the perovskite phases is also reversible by switching the gating voltage to +1.8 V. Thus, with the ILG, we achieve the reversible phase transformations among three phases, and indeed the phase transformations can also be controlled between the brownmillite phase and others (**Extended Data Figures 2i, j**). It is important to note that these transformations are nonvolatile, as confirmed with the *ex-situ* XRD measurements without the gating voltage (**Figure 1d**), which makes all the *ex-situ* studies possible and provides broader range of applications. From the comparison of the *ex-situ* detailed XRD measurements, the similar super-structure diffractions between the $SrCoO_{2.5}$ and phase A (green and blue curves respectively in **Figure 1d**) suggest an alternating arrangement of the oxygen polyhedral layers[13] in these two phases, which however does not exist in the perovskite $SrCoO_{3-\delta}$ phase (red curve in **Figure 1d**). Reciprocal space mapping and rocking curve measurements (**Extended Data Figure 1**) prove that the films remain of high crystalline quality throughout the ILG. Additionally, the effective and generic natures of this approach are further extended with the controlled experiments on films with different thicknesses and strain states (**Extended Data Figure 3**).

To investigate the valence states of the Co cations in different phases, soft X-ray absorption spectroscopy (sXAS) was performed at the Co *L*-edge and oxygen *K*-edge (**Methods**). The peak positions of the Co *L*-edge (**Figures 2a**) shift toward higher energy following the sequence of phase A, $SrCoO_{2.5}$ to $SrCoO_{3-\delta}$, suggesting the increase of valence states and confirming the excellent oxygen stoichiometry ($\delta < 0.1$) of the latter two phases[24]. Furthermore, a straightforward comparison with the reference CoO spectrum confirms that the Co cations in phase A are dominated by the

+2 oxidation state[25]. The O-*K* sXAS results (**Figure 2b**) show a significant reduction of the Co-O hybridization feature with the transition from $SrCoO_{3-\delta}$ to $SrCoO_{2.5}$, which is consistent with the previous study[24]. However, the loss of the hybridization feature in phase A is in sharp contrast to the conventionally reduced $SrCoO_x$, thus establishing itself as a distinct compound from others. Nevertheless, the strong suppression of the sXAS hybridization features~~similar phenomenon~~ was indeed observed in the~~a~~ Li_xFePO_4 system upon lithiation (Li-ion intercalation)[26].

Subsequently, the atomic structural analysis of the phase A with the high-resolution scanning transmission electron microscopy (**Figure 2c**) reveals the alternating stacking of oxygen octahedral and tetrahedral layers with periodic modulations of the vertical Sr-Sr atomic distance (**Figure 2d**), consistent with XRD results. Specifically, compared with the $SrCoO_{2.5}$ (**Methods** and **Extended Data Figure 4a**), the Sr-Sr atomic distance of the phase A is increased from ~4.3 Å to ~4.7 Å in the tetrahedral sub-layers, but remains nearly unchanged in the octahedral sub-layers. This observation suggests that the phase transformation between the $SrCoO_{2.5}$ and phase A is mainly associated with the tetrahedral sub-layers.

We note that the oxygen extraction and hydrogen insertion form two possible mechanisms for the reduction of the Co ions from Co^{3+} ($SrCoO_{2.5}$) to Co^{2+} (phase A). If oxygen extraction is the dominant mechanism, it is reasonable to assume the chemical formula of phase A to be $SrCoO_2$. **Extended Data Figures 5a-c** illustrates three possible crystalline structures of the $SrCoO_2$ based on the first-principles calculations. However, all calculated structures show that the octahedral layers are dramatically deformed into either tetragonal or planar coordination[14], which are inconsistent with the experimental results. Indeed, our energy dispersive x-ray spectra measurements (**Extended Data Figure 4e**) suggest that the oxygen loss is negligible during the phase transformation from the $SrCoO_{2.5}$ phase to phase A. On the other hand, secondary ion mass spectrometry (SIMS) measurements (**Figure 2e**) show the presence of pronounced hydrogen signal in the film when tuned to the phase A, with the estimated hydrogen concentration for $SrCoO_{2.5}H_y$ to be y~1.14□0.25 (see **Methods**). Thus, we can identify the hydrogen insertion as the dominant mechanism

for the transformation, and tentatively assign the corresponding chemical formula of the phase A to be $SrCoO_{2.5}H$, assuming the +1 state of hydrogen ions (H^+). To testify this scenario and further elaborate the crystalline structure, the first-principles calculations (**Extended Data Figures 5d-g)** were performed and a lowest energy crystalline structure with H^+ bonded to the apical O^{2-} in tetrahedral layers is suggested (the right panel of **Figure 1c** and inset of **Figure 2c**). The optimized crystal structure of $SrCoO_{2.5}H$ shows a larger structural modulation of both vertical and lateral Sr-Sr atomic distances, as presented in **Figure 2d** and **Extended Data Figure 4c**, respectively, in good agreement with the experimental results. Moreover, the presence of the H^+ in the $SrCoO_{2.5}H$ phase can be further confirmed by the dramatic variation of the peak features of the oxygen *K*-edge XAS spectra around 533-540 eV, where is know for the hydroxyl features in sXAS[27].

Thus, combing the extensive experimental and theoretical investigations, we revealed the exotic crystalline structure in the $SrCoO_{2.5}H$ phase, in which the H^+ ion insertion leads to a large positive structural expansion. This is in strong contrast to the structures of previously discovered transition metal oxyhydrides (e.g. $LaSrCoO_3H_{0.7}$[16], $BaTiO_{3-x}H_x$[17], $SrCoO_xH_y$[28], etc.) through thermal annealing in reducing agents, in which the hydride ions (H^-) replace oxygen ions with the negative structural expansion. Furthermore, our $SrCoO_{2.5}H$ phase forms a thermal equilibrium state in air at room temperature (**Extended Data Figure 6**), while the hydrogenated VO_2 phase gradually returns back to the dehydrogenated phase[18].

We want to emphasize that although the unipolar (involving only the O^{2-} ion) phase transformation between the $SrCoO_{2.5}$ and $SrCoO_{3-\delta}$ have already been achieved with the thermal annealing[12] and electrochemical redox reaction[5], the current study demonstrates a conceptually new pathway to achieve the deterministic and reversible electric-field control of the tri-state phase transformation through the selective bipolar and dual-ion (both O^{2-} and H^+) switch, as summarized in **Figure 1c**.

Armed with the knowledge of the crystalline structures and elemental compositions for all three phases, we identify the electrolysis of water as the most promising origin for O^{2-} and H^- ions (**Methods** and **Extended Data Figures 7a, b**). Indeed, we were

able to demonstrate the liquid gating induced phase transformations with several ionic liquids, which all possess considerable amount of water residual (**Extended Data Figure 8**). Furthermore, by doping the ionic liquids with heavy water, using SIMS measurements, we were able to trace a clear deuterium (D) signal uniformed distributed inside the $SrCoO_{2.5}H$, which nails down the water inside ionic liquid as the origin of the ions for the phase transformations (**Methods and Extended Data Figures 7c, d**).

Owing to the changes of both valence states and crystal structures through the phase transformation, we observe a fascinating electrochromic effect with electrically switchable spectra optical transparency. Obvious color differences of the three phases can be seen in photographs presented in **Figure 3a**. Both the *ex-situ* quantitative optical full range (**Figure 3b**) and *in-situ* transient (**Extended Data Figure 9**) transmittance measurements show that the $SrCoO_{2.5}H$ phase has great transmittance in both the visible-light and infrared regions, while the $SrCoO_{2.5}$ transmits mainly in the infrared region and the $SrCoO_{3-\delta}$ blocks the entire region. Thus, with the electric-field controlled phase transformation among these three phases, we demonstrate an interesting tri-state electrochromic effect with the superior large tunable transmittance regions covering the whole infrared and visible-light (dual-band) regions, which holds promising applications for smart windows[2, 9] as proposed schematically in the inset of **Figure 3b**.

Such an intriguing capability is attributed to the different direct band gaps of these three phases. Through fitting of the optical absorption spectra (**Figure 3c**), the direct band gaps of the $SrCoO_{2.5}$ and $SrCoO_{2.5}H$ phases are extracted to be 2.12 and 2.84 eV respectively, which leads to the large difference of the optical transmittance in the visible-light region. The large increase of band gap of the $SrCoO_{2.5}H$ phase is attributed to the weaker *p-d* hybridization as revealed by the oxygen *K* pre-edge XAS study (**Figure 2b**), and is further confirmed with the first-principles calculations (**Extended Data Figure 10**). The electrical transport measurements provide further evidence of the associated electronic structure modulation (**Figure 3d**). The change of resistivities by six orders of magnitude among these three phases and their

temperature dependences confirm that $SrCoO_{3-\delta}$ is a good metal, while $SrCoO_{2.5}$ and $SrCoO_{2.5}H$ are both insulators.

Interestingly, the electric-field controlled phase transformation is also accompanied with the change of the magnetic ground states. Macroscopic magnetic measurements (**Figures 4a and 4b**) show a ferromagnetic state in the $SrCoO_{3-\delta}$ phase with the saturated magnetization of 2.4 μ_B/Co (T_c ~240 K) and a minimal magnetic response from the antiferromagnetic $SrCoO_{2.5}$ phase (T_N ~537 K) [13], both consistent with the previous experimental results[12]. Surprisingly, the newly discovered $SrCoO_{2.5}H$ phase shows a well-defined magnetic hysteresis loop with the saturated moment of 0.6 μ_B/Co (T_c ~125 K). The magnetic ground states of these three phases were further investigated by X-ray magnetic circular dichroism (XMCD) measurements (**Figure 4c**), which provide direct and element-specific information of magnetism[29]. The clear XMCD signals of both the $SrCoO_{3-\delta}$ and $SrCoO_{2.5}H$ as compared with the non-detectable XMCD in the $SrCoO_{2.5}$ provide the solid evidence for the changes of magnetic ground states through the phase transformation.

Corresponding to the different magnetic ground states of these three phases, an intriguing tri-state magnetoelectric effect[11] can be obtained. Due to the rich magnetic phase diagram of this system, several kinds of magnetic transition could be realized at different temperature regions, as summarized in **Figure 4d**. We note that at the room temperature region, the $SrCoO_{2.5}$ is antiferromagnetic, while the other two are paramagnetic. Thus the phase transformation between $SrCoO_{2.5}$ and others would be accompanied with the magnetic transition between the antiferromagnetic and the paramagnetic states, which is equivalent to the turn/off of the antiferromagnetism. Clearly the current study provides a simpler and more practical method to achieve the electric field control of antiferromagnetism at room temperature, as compared with that obtained in the multiferroic with coupled ferroelectricity and antiferromagnetism through sophisticated ferroelectric domain manipulations[30].

References

1. Tarascon, J. M. & Armand, M. Issues and challenges facing rechargeable lithium batteries. *Nature* **414**, 359-367 (2001).
2. Granqvist, C. G. Electrochromics for smart windows: Oxide based thin films and devices. *Thin Solid Films* **546**, 1-38 (2014).
3. Steele, B. C. H. & Heinzel, A. Materials for fuel-cell technologies. *Nature* **414**, 345-352 (2001).
4. Jeong, J. *et al.* Suppression of metal-insulator transition in VO_2 by electric field-induced oxygen vacancy formation. *Science* **339**, 1402–1405 (2013).
5. Katase, T., Suzuki, Y. & Ohta, H. Reversibly switchable electromagnetic device with leakage-free electrolyte. *Adv. Electron. Mater.* **2**, 1600044 (2016).
6. Close, T., Tulsyan, G., Diaz, C. A., Weinstein, S. J. & Richter, C. Reversible oxygen scavenging at room temperature using electrochemically reduced titanium oxide nanotubes. *Nat. Nanotech.* **10**, 418-422 (2015).
7. Ji, H., Wei, J. & Natelson, D. Modulation of the electrical properties of VO_2 nanobeams using an ionic liquid as a gating medium. *Nano. Lett*. **12**, 2988-2992 (2012).
8. Shibuya, K., & Sawa, A. Modulation of metal–insulator transition in VO_2 by electrolyte gating-induced protonation. *Adv. Electron. Mater.* **2**, 1500131 (2016).
9. Llordés, A., Garcia, G., Gazquez, J. & Milliron D. Tunable near-infrared and visible-light transmittance in nanocrystal-in-glass composites. *Nature* **500**, 323-326 (2013).
10. Lu, Q. & Yildiz, B. Voltage-controlled topotactic phase transition in thin-film $SrCoO_x$ monitored by in situ X-ray diffraction. *Nano Lett*. **16**, 1186-1193 (2016).
11. Schmid, H. Multi-ferroic magnetoelectrics. *Ferroelectrics* **162**, 317 (1994).
12. Jeen, H. *et al.* Reversible redox reactions in an epitaxially stabilized $SrCoO_x$ oxygen sponge. *Nat. Mater.* **12**, 1057-1063 (2013).
13. Muñoz, A. *et al*. Crystallographic and magnetic structure of $SrCoO_{2.5}$ brownmillerite: Neutron study coupled with band-structure calculations. *Phys. Rev. B* **78**, 055504 (2008).
14. Tsujimoto, Y. *et al.* Infinite-layer iron oxide with a square-planar coordination. *Nature* **450**, 1062-1065 (2007).
15. Zhou, Y. *et al.* Strongly correlated perovskite fuel cells. *Nature* **534**, 231-234 (2016).
16. Hayward, M. *et al.* The hydride anion in an extended transition metal oxide array: $LaSrCoO_3H_{0.7}$. *Science* **295**, 1882-1884 (2002).
17. Kobayashi, Y. *et al.* An oxyhydride of $BaTiO_3$ exhibiting hydride exchange and electronic conductivity. *Nat. Mater.* **11,** 507-511 (2012).
18. Yoon, H. *et al*. Reversible phase modulation and hydrogen storage in multivalent VO_2 epitaxial thin films. *Nat. Mater*. **15**, 1113-1119 (2016).
19. Simon, P. & Gogotsi Y. Materials for electrochemical capacitors. *Nat. Mater.* **7**, 845-854 (2008).
20. Ueno, K. *et al*. Electric-field-induced superconductivity in an insulator. *Nat. Mater.* **7**, 855-858 (2008).
21. Yamada Y. *et al.* Electrically induced ferromagnetism at room temperature in cobalt-doped titanium dioxide. *Science* **332**, 1065-1067 (2011).
22. Yuan, H. T. *et al.* Electrostatic and electrochemical nature of liquid-gated electric-double-layer transistors based on oxide semiconductors. *J. Am. Chem. Soc.* **132**, 18402-18407 (2010).
23. Mitra, C., Meyer, T., Lee, H. N. & Reboredo, F. A. Oxygen diffusion pathways in brownmillerite $SrCoO_{2.5}$: Influence of structure and chemical potential. *J. Chem. Phys.* **141**, 084710 (2014).

24. Karvonen, L. *et al.* O-*K* and Co-*L* XANES study on oxygen intercalation in perovskite $SrCoO_{3-\delta}$. *Chem. Mater.* **22**, 70-76 (2009).
25. Magnuson, M., Butorin, S. M., Guo, J. H. & Nordgren, J. Electronic structure investigation of CoO by means of soft x-ray scattering. *Phys. Rev. B* **65**, 205106 (2002).
26. Liu, X. S. *et al*. Why $LiFePO_4$ is a safe battery electrode: Coulomb repulsion induced electron-state reshuffling upon lithiation. *Phys. Chem. Chem. Phys.* **17**, 26369-26377 (2015).
27. Shan, X. Q. *et al*. Bivalence Mn_5O_8 with hydroxylated interphase for high-voltage aqueous sodium-ion storage. *Nat. Commun.* **7**, 13370 (2016).
28. Katayama, T. *et al.* Topotactic synthesis of strontium cobalt oxyhydride thin film with perovskite structure. *AIP Adv*. **5**, 107147 (2015).
29. Chen, C. T. *et al.* Experimental confirmation of the x-ray magnetic circular dichroism sum rules for iron and cobalt. *Phys. Rev. Lett.* **75**, 152-155 (1995).
30. Zhao, T. *et al.* Electrical control of antiferromagnetic domains in multiferroic $BiFeO_3$ films at room temperature. *Nat. Mater.* **5**, 823-829 (2006).

Acknowledgement: This study was financially supported by the National Basic Research Program of China (2015CB921700, 2015CB921002, 2016YFA0301004), National Natural Science Foundation of China (11274194, 51561145005) and Initiative Research Projects of Tsinghua University (20131089195, 20141081116). L. G acknowledges support from the National Program on Key Basic Research Project (2014CB921002) and The Strategic Priority Research Program of Chinese Academy of Sciences (Grant No. XDB07030200) and National Natural Science Foundation of China (51522212, 51421002, 51672307). The Advanced Light Source is supported by the U.S. Department of Energy under Contract No. DE-AC02-05CH11231.

Author contribution: N.L., Y. W., Z. D. and Z. L. fabricated the thin films. N.L. performed the ionic liquid gating, X-ray diffraction, magnetic and optical measurements with H. L., Y. W., S. Y. and M. W. P. Z. performed the theoretical analysis and calculations under the supervision of J. W. Q. Z. performed the scanning transmission electron microscopy measurements under the supervision of L. G. and C. N. R. Q., J. G. and M. Y. performed the room temperature X-ray absorption measurements under the supervisions of S. Z. and W. Y. Q. H., J. G. and E. A. performed the low temperature X-ray magnetic circular dichroism measurements. D. Z., H. L. and N. L. performed the electrical transport measurements. Y. T discussed the results. N. L. and P. Y. wrote the manuscript. The study was conceived and guided by P. Y. All authors discussed results and commented on the manuscript.

Competing financial interest: The authors declare no competing financial interests.

Figures and Captions

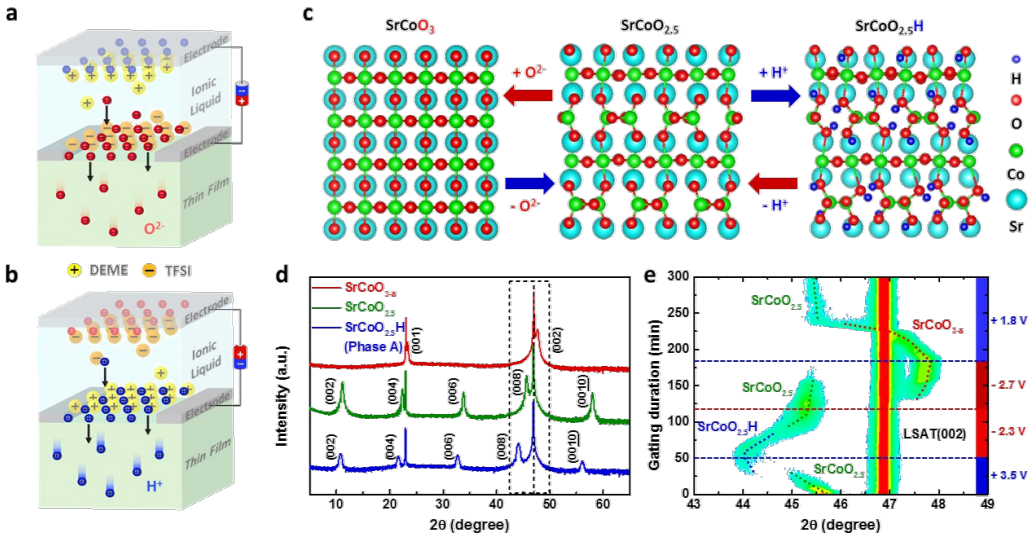

Figure 1 | Electric-field control of tri-state phase transformation between $SrCoO_{2.5}$, $SrCoO_{3-\delta}$ and phase A ($SrCoO_{2.5}H$). Schematic diagrams of the transport and storage of **(a)** oxygen and **(b)** hydrogen ions with negative and positive external gating voltages in an ionic liquid gating device, respectively. For negative voltage, the internal electric field formed by the ionic liquid gating can drive the negative charged O^{2-} ions into the films to fill in the oxygen vacancies. While, the positive voltage can lead to the insertion of positive charged H^{+} ions. The reversed gating can induce the extraction of the corresponding ions for both cases. **c,** Schematic illustrations of the reversible phase transformation of $SrCoO_{2.5}$ through the electric-field selectively controlled dual-ion (O^{2-} and H^{+}) switch. The crystal structures were obtained from the first principles calculations. The red and blue arrows represent negative and positive voltages, respectively. **d,** Detailed X-ray diffraction ***θ-2θ*** scans of the perovskite $SrCoO_{3-\delta}$ (top), brownmillerite $SrCoO_{2.5}$ (middle) and phase A ($SrCoO_{2.5}H$) (bottom) films grown on $(LaAlO_3)_{0.3}$-$(SrAl_{0.5}Ta_{0.5}O_3)_{0.7}$ (LSAT) (001) substrates. **e,** *In-situ* X-ray diffraction results zoomed-in around the LSAT (002) peaks under the ionic liquid gating with the controlled gating voltages. The strongest peak at ~ 46.9° is from the substrate, and the peaks from $SrCoO_{2.5}$, phase A ($SrCoO_{2.5}H$) and $SrCoO_{3-d}$ are marked by green, blue and red broken lines.

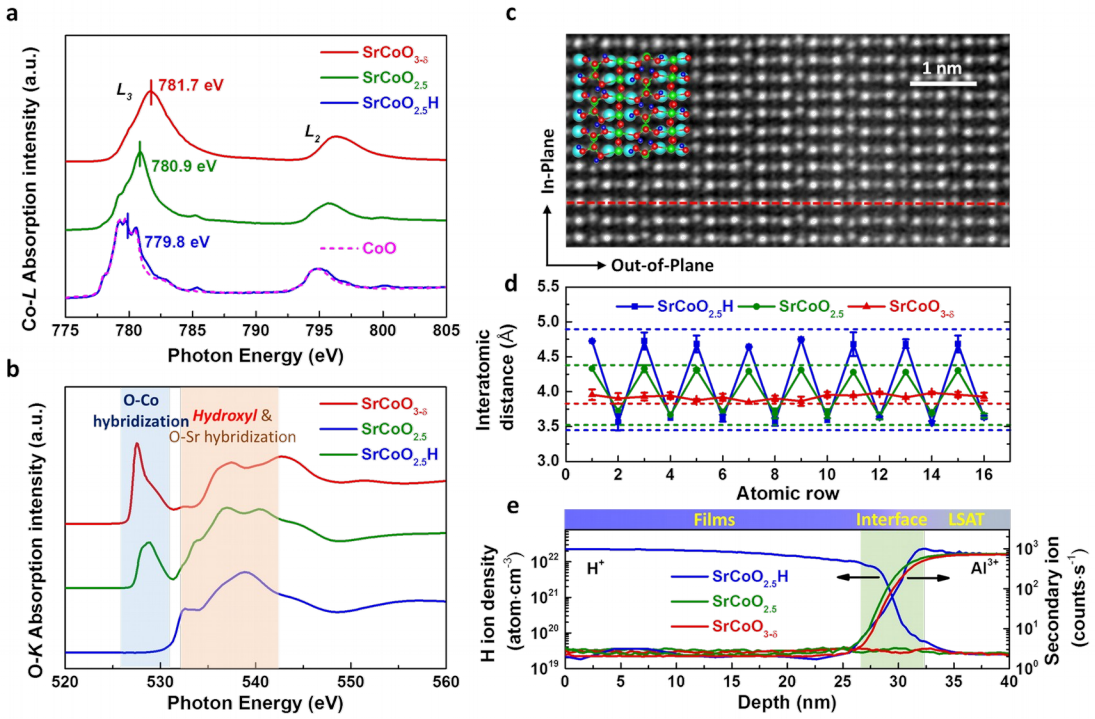

Figure 2 | Identification of the newly discovered phase A ($SrCoO_{2.5}H$). Comparison of soft X-ray absorption spectra of $SrCoO_{3-\delta}$, $SrCoO_{2.5}$ and phase A ($SrCoO_{2.5}H$) at **(a)** Co *L*-edges and **(b)** *O K*-edges, from which the valance states of Co ~~atoms~~ and the hybridization between O *2p* and Co *3d* can be clarified. **c,** High-angle annular dark field scanning transmission electron microscopy (HAADF-STEM) measurements of the phase A. The zone axis is along the [110] direction of LSAT substrate. The calculated crystal structure of the $SrCoO_{2.5}H$ is shown for comparison. The red broken line was used to obtain the corresponding Sr-Sr interatomic distances. **d,** Comparison of the experimental results of the out-of-plane Sr-Sr interatomic distances among three different phases (symbols) with the theoretical calculated results (dashed lines). **e,** Depth profiles of the H and Al ions on all three different phases measured with the secondary ion mass spectrometry. The signal of the Al^{3+} ions from the LSAT substrate was employed as a marker for the position of the interface. Large amount of H^+ ions is uniformly distributed in the film when it is tuned to the $SrCoO_{2.5}H$ phase. While for the other two phases, the H^+ signal is only comparable to the substrate.

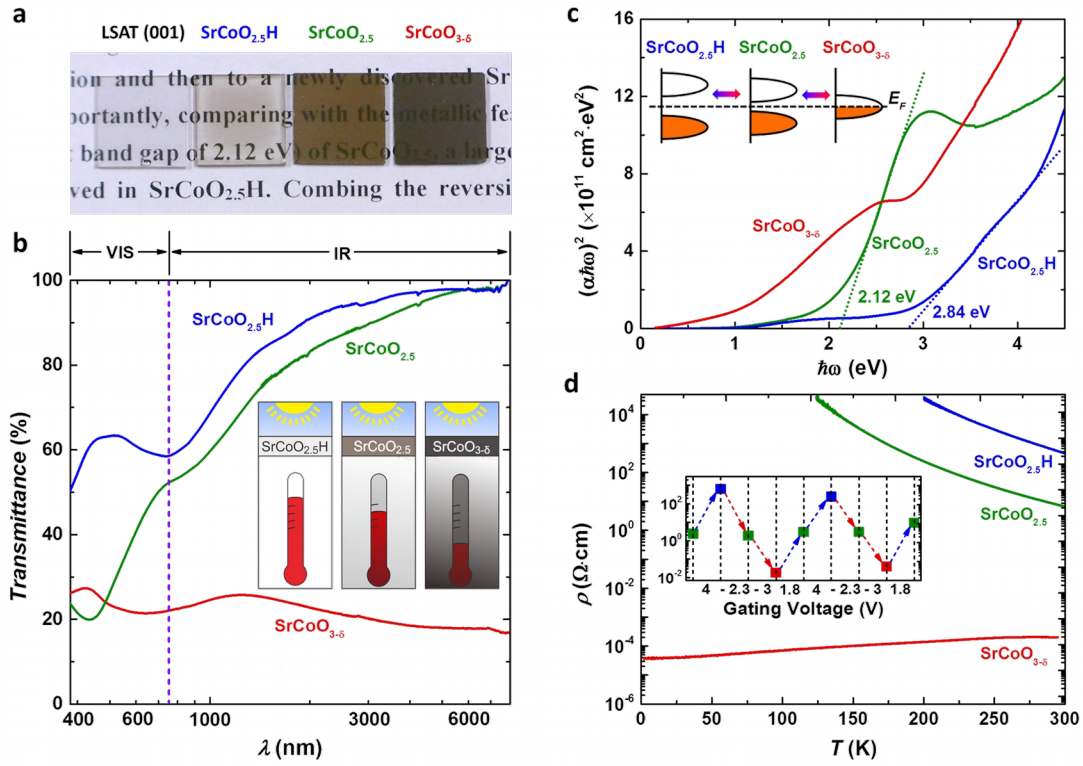

Figure 3 | Tri-state dual-band electrochromic effect and electrically controlled metal-insulator transition. a, Comparison of optical photographs of $SrCoO_{2.5}H$, $SrCoO_{2.5}$ and $SrCoO_{3-\delta}$ thin films with the thickness of 50 nm grown on double-side polished LSAT substrates. The size of the samples is 10 mm by 10 mm. **b,** Optical transmission spectra of samples through the phase transformation. Inset shows a schematic proposal of the smart window based on the tunable optical transmittance. **c,** $(\alpha\omega)^2$ vs. ω plot of the absorption spectra. The inset shows the schematic band alignments for these three phases. To estimate the direct band gaps of the $SrCoO_{2.5}$ and $SrCoO_{2.5}H$, the absorption data were fitted with the equation of $(\alpha\hbar\omega)^2 = A(\hbar\omega - E_g)$, where where α, $\hbar\omega$ and E_g are the optical absorption, photon energy and the size of the direct band gap, respectively. **d,** Temperature dependence of the electrical resistivity. Inset shows a experimental demonstration of the concept of the tri-state resistive switch.

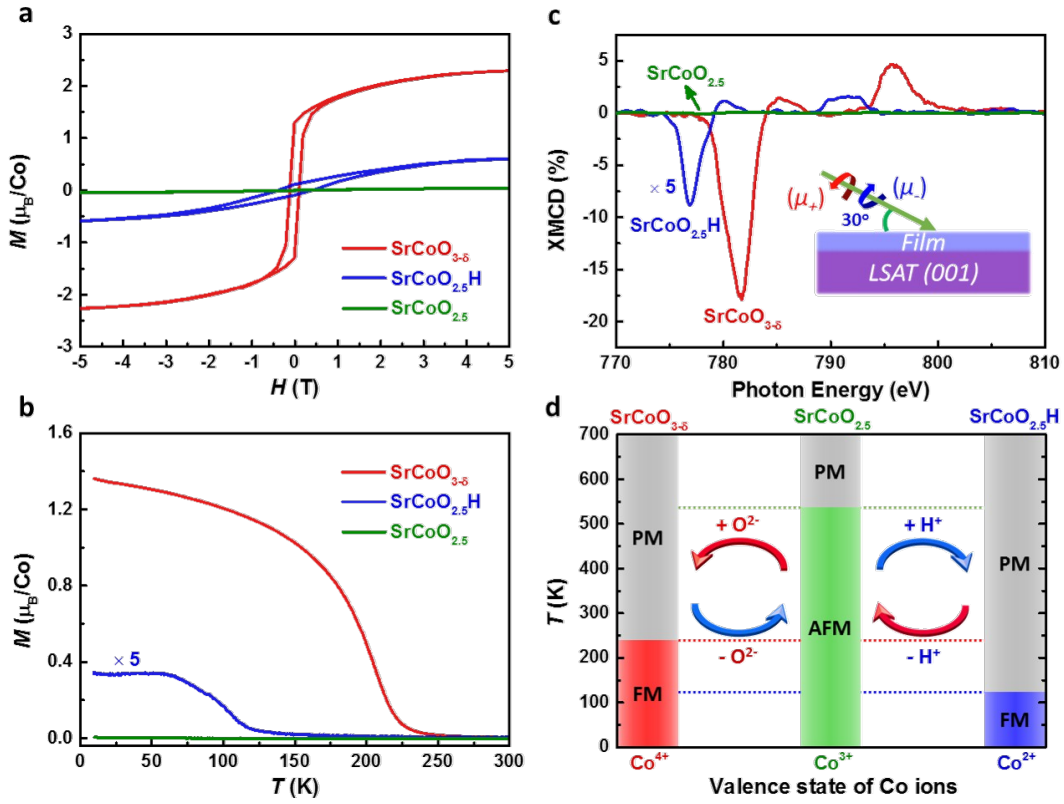

Figure 4 | Tri-state magnetoelectric coupling with the electric-field selectively controlled dual-ion switch. a, Magnetic hysteresis loops measured at 10 K. The magnetic field is applied along the in-plane [100] direction of the LSAT substrates. **b,** Temperature-dependent magnetization measurements with filed cooling at 0.1 T. **c,** X-ray magnetic circular dichroism spectra at Co $L_{2,3}$ edges taken at 20 K with the magnetic field of 1.5 T applied along the incident light direction. Inset shows the schematic configuration of the experiments. **d,** Schematic illustration of the magnetoelectric effects at different temperature regions. The distinct magnetic and electronic ground states for these three phases lead to intriguing magnetic transitions and magnetoelectric effects at different temperature regions.